
^{11}C -GR103545, a Radiotracer for Imaging κ -Opioid Receptors In Vivo with PET: Synthesis and Evaluation in Baboons

Peter S. Talbot, MD¹; Raj Narendran, MD¹; Eduardo R. Butelman, PhD²; Yiyun Huang, PhD^{1,3}; Kim Ngo, BS¹; Mark Slifstein, PhD¹; Diana Martinez, MD¹; Marc Laruelle, MD^{1,3}; and Dah-Ren Hwang, PhD¹

¹Department of Psychiatry, Columbia University College of Physicians and Surgeons and the New York State Psychiatric Institute, New York, New York; ²Laboratory on the Biology of Addictive Diseases, Rockefeller University, New York, New York; and ³Department of Radiology, Columbia University College of Physicians and Surgeons and the New York State Psychiatric Institute, New York, New York

Brain κ -opioid receptors (ORs) may be involved in several pathologic conditions, such as addiction, psychosis, and seizures. (\pm)-4-Methoxycarbonyl-2-[(1-pyrrolidinylmethyl)-1-[(3,4-dichlorophenyl)acetyl]-piperidine (GR89696) is a potent and selective κ -OR agonist. The (-)-isomer, GR103545, is the active enantiomer of GR89696. The aim of this study was to characterize the potential of ^{11}C -GR103545 to image κ -OR in vivo with PET. **Methods:** Brain uptake of ^{11}C -GR103545 was studied in baboons under control conditions and after blockade by naloxone (1 mg/kg intravenously). Uptake of the racemic ^{11}C -GR89696 and of the inactive enantiomer (+)- ^{11}C -GR89696 was also evaluated. Regional total distribution volumes were derived using the arterial input function and a 2-tissue-compartment model. **Results:** ^{11}C -GR103545 showed excellent brain penetration and uptake kinetics, with significant washout observed within the time frame of the PET experiment. Naloxone pretreatment did not affect cerebellar total distribution volume and reduced total distribution volume in other regions to a level comparable to that in the cerebellum. The regional pattern of ^{11}C -GR103545 binding potential was consistent with the distribution of κ -OR in primate brain, with highest levels observed in anterior cortical regions (prefrontal cortex and cingulate cortex) and striatum. In most regions, the specific-to-nonspecific equilibrium partition coefficient (V_3'') ranged from 1 to 2, predicting reliable quantification. ^{11}C -GR103545 V_3'' values were approximately double the ^{11}C -GR89696 V_3'' values, whereas (+)- ^{11}C -GR89696 V_3'' values were negligible, demonstrating the enantiomeric selectivity of the binding and the advantage of using the pure active enantiomer for PET studies. **Conclusion:** ^{11}C -GR103545 is a promising PET radiotracer for imaging the κ -OR.

Key Words: κ -opioid receptor; (-)- ^{11}C -4-methoxycarbonyl-2-[(1-pyrrolidinylmethyl)-1-[(3,4-dichlorophenyl)acetyl]-piperidine; PET; baboon

J Nucl Med 2005; 46:484–494

Opioid receptors (ORs) belong to the superfamily of G-protein-coupled receptors and are generally classified into at least 3 subtypes: δ (enkephalin-preferring), κ (dynorphin-preferring), and μ (morphine-preferring; β -endorphin may be a major endogenous ligand at this receptor) (1). These different receptor subtypes have been isolated, cloned, and pharmacologically characterized (2). In general, agonists at the μ - and δ -receptor sites are rewarding and reinforcing, whereas agonists at the κ -receptor site are aversive.

In humans, the κ -OR is the most abundant brain OR and is widely distributed in forebrain, midbrain, and brain stem structures. Its protein and messenger RNA are concentrated in deeper layers of the neocortex (particularly temporal, parietal, and frontal cortices), striatum, and thalamus, with lower levels in amygdala, hippocampus, occipital cortex, and cerebellum (3–5). A similar distribution is seen in the nonhuman primate brain (6,7).

One gene coding for the κ -OR has been identified in humans (3). However, radioligand binding studies have suggested the existence of κ -OR subtypes with different ligand binding and anatomic distribution profiles. Thus, κ_1 - and κ_2 -binding sites have been described in rodents, nonhuman primates, and humans (8–10). The cloned human κ -OR appears pharmacologically similar to the κ_1 -subtype (11), but κ_1 -receptors appear to compose the minority of κ -OR in primates (9). The κ_2 -receptor, which is the predominant subtype in primates (8), may represent the heterodimerization of 2 fully functional ORs (κ and δ), resulting in a new receptor that exhibits ligand binding and functional properties distinct from those of either receptor (12). Other lines of evidence suggest that these different binding subtypes may, in fact, represent different affinity states of the same receptor (13,14).

The κ -OR has been implicated in several clinical brain disorders, including substance (particularly psychostimulant) abuse (15), epilepsy (16), Tourette's syndrome (17),

Received May 18, 2004; revision accepted Aug. 12, 2004.
For correspondence or reprints contact: Peter S. Talbot, MD, Division of Functional Brain Mapping, New York State Psychiatric Institute, Unit 31, 1051 Riverside Dr., New York, NY 10032.
E-mail: pst2001@columbia.edu

and Alzheimer's disease (18). Of additional possible clinical significance is the observation that certain κ -OR agonists are extremely potent hallucinogens (19) and a report that hallucinations in chronic schizophrenia are ameliorated by high-dose naloxone, a relatively nonselective opiate receptor antagonist that antagonizes κ -OR at higher doses (20). In addition, κ -OR agonism promotes (and antagonism reduces) neurodegeneration in models of central nervous system injury and ischemia (21). Thus, the ability to image κ -OR would be important in characterizing the involvement of κ -transmission in these conditions.

Several OR radiotracers are currently available for PET in humans, including ^{11}C -carfentanil (22), ^{11}C -diprenorphine (23), ^{11}C -buprenorphine (24), ^{18}F -cyclofoxy (25), and ^{11}C -naltrindole (26), but none is selective for the κ -OR.

(\pm)-4-Methoxycarbonyl-2-[(1-pyrrolidinylmethyl)-1-[(3,4-dichlorophenyl)acetyl]-piperidine (GR89696) is a novel, highly potent, and selective κ -OR agonist (27). The (–)-isomer, (–)-4-methoxycarbonyl-2-[(1-pyrrolidinylmethyl)-1-[(3,4-dichlorophenyl)acetyl]-piperidine, also known as GR103545, is the more potent optical isomer of GR89696. GR89696 is centrally penetrating, with a log P value of 3.14 (28), and has potent antinociceptive, sedative, and diuretic effects (28–31). K_i values for GR89696 κ_1 - and κ_2 -receptor binding are in the low nanomolar or subnanomolar range. GR89696 displaces ^3H -bremazocine binding (representing both κ_1 - and κ_2 -receptors) with a K_i of 2.3 nmol/L in the guinea pig (32) and 1.15 nmol/L in the rhesus monkey (33). K_i values at the κ_1 - and κ_2 -receptors selectively were 0.5 nmol/L and 6.3 nmol/L, respectively (32).

In 1999, Ravert et al. (34) reported the radiolabeling of the racemic ^{11}C -GR89696. Studies in mice supported the potential of this radiotracer for PET imaging of κ -OR. More recently, Ravert et al. (35) reported the ^{11}C -labeling and in vivo evaluation of both optical isomers of GR89696 in mice. Uptake of the active isomer, ^{11}C -GR103545, correlated with the known distribution of κ -OR. On the other hand, the inactive isomer, (+)-GR89696, showed a homogeneous brain uptake.

The present study was undertaken to further evaluate the potential of the active isomer, ^{11}C -GR103545, as a PET radiotracer to image and quantify κ -OR. PET studies were performed on baboons (*Papio anubis*) to characterize the kinetics and distribution of ^{11}C -GR103545 in the primate brain. Studies were performed under both control and blocked conditions to demonstrate the specificity of the uptake. Kinetic analyses using the arterial input function were developed to quantify in vivo κ -OR availability. The distribution of ^{11}C -GR103545 in the baboon brain was compared with the distribution of the racemic ^{11}C -GR89696 and of the inactive enantiomer (+)- ^{11}C -GR89696, to demonstrate enantiomeric selectivity. The distribution of ^{11}C -GR103545 in the baboon brain was also compared with the distribution of the selective μ -OR agonist radiotracer ^{11}C -carfentanil.

MATERIALS AND METHODS

General

The chiral high-performance liquid chromatography (HPLC) column was a Chiralcel-OD (4.6 \times 250 mm; Daicel). The analytic HPLC system was equipped with a Rheodyne injector (Alltech) with a 2-mL sample loop, an ODS-3 column (5 μm , 250 \times 4.6 mm; Phenomenex), a PDA detector (Waters), and a flow-cell γ -detector (Bioscan). The semipreparative HPLC system comprised an ODS-Prep column (10 μm , 250 \times 10 mm; Phenomenex), an ultraviolet detector (model 450; Alltech), and a pin diode γ -detector (Bioscan). For metabolite analysis, a ODS-Prep column (10- μm , 250 \times 4.6 mm; Phenomenex), a flow-cell γ -detector (Bioscan), and a fraction collector (Spectra/Chrom CF-1; Fisher Scientific) were used.

^1H -nuclear magnetic resonance (NMR) spectra were recorded on DRX300 or DRX400 NMR instruments (Bruker). Optical rotations were measured using a P-1010 digital polarimeter with a halogen lamp and a 1-cm sample cell (Jasco Inc.).

Chemistry

Numbered compounds refer to the numbering scheme in Figure 1. GR103545 (compound 8) and its optically pure precursor, (–)-7, were prepared from D-serine according to a modification of a published procedure (31). The reaction conditions are shown in Figure 1. The most critical step of the synthesis is the preparation of the optically pure (–)-6, which involves the formation of an intermediate aldehyde from compound 5, followed by a reductive amination reaction. To avoid the undesired racemization, a solution of anhydrous HCl in methanol was used to adjust the pH of the reaction mixture to 6. The optical purity of (–)-6 was further confirmed after its conversion to the optically pure GR103545.

The optical purity of the synthetically obtained GR103545 and its chiral precursor, (–)-7, were confirmed by both optical rotation measurements and chiral HPLC analysis (Fig. 2). Our measured optical rotations of GR103545 agreed with those reported in the literature (31,35).

The chiral HPLC procedure was that used by Ravert et al. (35) for the separation of GR103545 from GR89695. A similar proce-

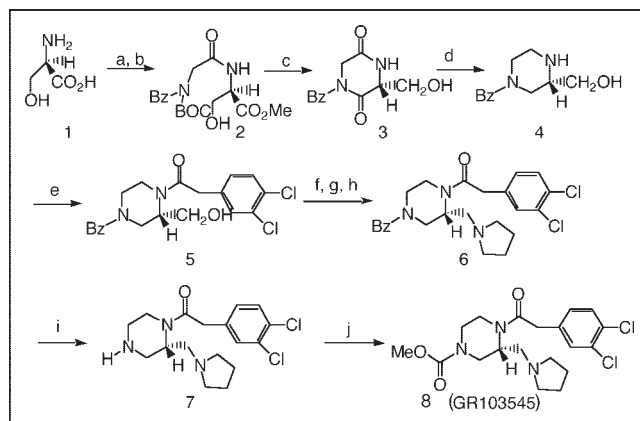


FIGURE 1. Preparation of GR103545 and the chiral precursor 7. Reaction conditions: (a) thionyl chloride (SOCl₂), methanol; (b) *N*-Boc-*N*-Bz-NBz-glycine, *N,N*-dicyclohexylcarbodiimide; (c) SOCl₂; (d) lithium aluminum hydride; (e) 3,4-dichlorophenylacetyl chloride; (f) dimethyl sulfoxide, oxalyl chloride, morpholine; (g) pyrrolidine, HCl/methanol, pH 6; (h) sodium cyanoborohydride; (i) H₂/Pd/C; (j) methyl chloroformate.

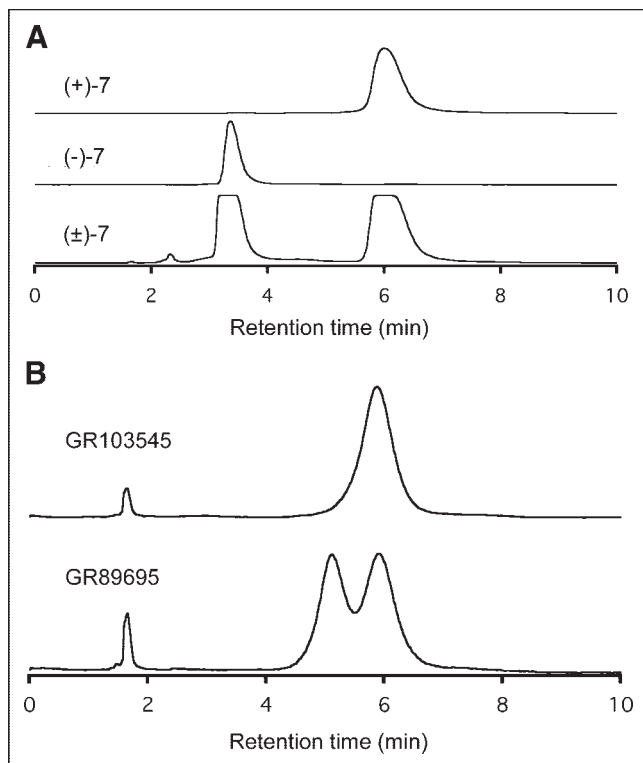


FIGURE 2. (A) Chiral HPLC separation of optical isomers of compound 7, showing *R*-(+)-isomer of 7, *S*-(-)-isomer of 7, and racemic (\pm) isomers of 7. HPLC conditions: column, Chiralcel OD (250 \times 4.6 mm); solvent, 25%:75%:0.01% isopropanol:hexane:diethylamine; flow rate, 2 mL/min. (B) Chiral HPLC separation of optical isomers of GR89695, showing GR103545 (the (-)-isomer) and GR89695 (the racemic isomers). HPLC conditions: column, Chiralcel OD (250 \times 4.6 mm); solvent, 20%:80%:0.01% isopropanol:hexane:diethylamine; flow rate, 2 mL/min.

cedure was used for the verification of the enantiomeric purities of the synthetically prepared GR103545 and compound 7. Figure 2A shows the baseline separation of both optical isomers of (\pm)-7. The first peak of the chiral HPLC corresponds to that of (-)-7 isomer. The same conditions were used to isolate the less active enantiomer, (+)-7, from the racemic (\pm)-7.

Similarly, the 2 optical isomers of GR89695 can be detected by the chiral HPLC method (Fig. 2B). The synthesized GR103545 showed a single peak with a retention time of 6.1 min (top line), indicating the high optical purity of the authentic GR103545.

Synthesis of (-)-1-[(3,4-Dichlorophenyl)Acetyl]-2-[(1-Pyrrolidinyl)Methyl]-Piperidine, (-)-7. A solution of (-)-1-[(3,4-dichlorophenyl)acetyl]-4-(phenylmethyl)-2-[(1-pyrrolidinyl)methyl]piperidine (0.293 g, 0.521 mmol), compound 6, in 8 mL of tetrahydrofuran:water (1:1) and 0.7 mL of concentrated HCl was hydrogenated (hydrogen balloon) over 10% palladium over charcoal (Pd/C) (0.14 g) at room temperature for 6 h. The solution was filtered through celite, and the filtrate was concentrated in vacuo. The residue was mixed with water (20 mL) and basified with sodium bicarbonate. The mixture was extracted twice with methylene chloride. The organic extracts were combined, dried over sodium carbonate, and concentrated in vacuo. The residue was purified by flash column chromatography on silica gel (100:5:1 methylene chloride:methanol:ammonium hydroxide) to give a col-

orless oil (0.16 g, 86%). $^1\text{H-NMR}$ (deuterated chloroform): 7.4 (br s, 2H), 7.15 (m, 1H), 4.4–4.8 (m, 1H), 3.4–3.9 (m, 3H), 2.4–3.3 (m, 12H), 1.5–2 (br s, 4H + water). $[\alpha]_{25} = -39.86^\circ$ ($c = 0.01756$ g/mL, CHCl_3). Chiral HPLC (20:80:0.01 isopropanol:hexane:diethylamine, 2 mL/min) showed the presence of only 1 isomer, with a retention time of 3.4 min.

Synthesis of (\pm)-1-[(3,4-Dichlorophenyl)Acetyl]-2-[(1-Pyrrolidinyl)Methyl]-Piperidine, (\pm)-7. (\pm)-1-[(3,4-dichlorophenyl)acetyl]-4-(phenylmethyl)-2-[(1-pyrrolidinyl)-methyl]piperidine (0.4 g, 0.712 mmol), concentrated HCl (0.85 mL), and Pd/C (0.15 g) in 22 mL of tetrahydrofuran:H₂O (1:1) were hydrogenated according to the procedure described above to give (\pm)-7 (0.24 g, 95%).

Isolation of (+)-1-[(3,4-Dichlorophenyl)Acetyl]-2-[(1-Pyrrolidinyl)Methyl]-Piperidine, (+)-7. (+)-7 was isolated by chiral HPLC using an analytic Chiralcel-OD and a solvent mixture of 25% isopropanol and 75% hexane with 0.01% diethylamine at a flow rate of 2 mL/min. The retention times for (-)- and (+)-7 were 3.4 and 6 min, respectively. (+)-7: $[\alpha]_{25} = +20.8^\circ$ ($c = 0.0048$ g/mL, CHCl_3).

Synthesis of GR103545, (-)-8. To a solution of (-)-7 (1.28 g, 3.596 mmol) and triethylamine (0.51 mL, 3.66 mmol) in methylene chloride at -10°C was added methyl chloroformate (0.278 mL, 3.598 mmol). The solution was stirred at -10°C for 50 min. A solution of aqueous sodium carbonate was added. The mixture was extracted with methylene chloride. The organic extracts were dried and concentrated in vacuo. The residue was purified by flash column chromatography on silica gel (100:5:0.5 methylene chloride:methanol:ammonium hydroxide) to give a colorless oil. Chiral HPLC (10:90:0.01 isopropanol:hexane:diethylamine, Chiralcel-OD, 2 mL/min) showed the presence of only 1 isomer, with a retention time of 6 min. $^1\text{H-NMR}$ (deuterated chloroform): 7.4 (m, 2H), 7.15 (m, 1H), 4.4–4.9 (m, 1H), 4–4.2 (m, 2H), 3.7–3.9 (m plus a strong s at 3.75, 4H), 2.4–3.6 (m, 10H), 1.7–1.9 (br s, 4H).

The oil was dissolved in methanol, and an equal molar amount of fumaric acid (0.192 g) was added. The solution was warmed in a water bath, and ethyl acetate was added to make the solution cloudy. After cooling, the salt was collected by filtration. Melting point = 184°C [b]– 185°C , $[\alpha]_{25} = -24.4^\circ$ ($c = 0.0023$ g/mL, H₂O).

Synthesis of GR89696, (\pm)-8. GR89696 was prepared from (\pm)-7 (0.2 g) according to the procedure described for the preparation of (-)-8. The colorless oil of the free base was converted to the HCl salt. Melting point = 171°C – 175°C .

Radiochemistry. ^{11}C was produced via the $^{14}\text{N}(p,\alpha)^{11}\text{C}$ nuclear reaction on a gas target (filled with 1% O₂ in N₂, 200 psi) using the Columbia University RDS112 negative ion cyclotron (CTI). ^{11}C was delivered into a 0.15-mL solution of lithium aluminum hydride (20 mg) in tetrahydrofuran (5 mL) at room temperature. After trapping, the solution was heated with a heat gun under a stream of argon to remove tetrahydrofuran. A 1% solution of water in diethyleneglycol butyl ether (1 mL) was added to the residue, and the mixture was heated with a heat gun under a stream of argon (25–30 cm³/min) to distill ^{11}C -methanol into methylene chloride (0.3 mL) in an ice bath. After the distillation, a solution of 20% phosgene in toluene (5 μL) was introduced. The solution was left at room temperature for 5 min, and a solution of (-)-7, the desmethylcarbonyl GR103545 (3 mg), and triethylamine (5 μL) in methylene chloride (0.3 mL) was introduced. The solution was heated at 50°C for 5 min and then evaporated to dryness. The residue was dissolved in 1 mL of acetonitrile and purified by semipreparative HPLC (25% acetonitrile and 75% 0.1

mol/L ammonium formate) at a flow rate of 8 mL/min. The desired tracer had a retention time of 11 min. The product fraction was mixed with 100 mL of water and passed through a C18 Sep-Pak (Waters). After washing with 10 mL of water, the Sep-Pak was eluted with 1 mL of ethanol to recover the tracer. A small portion of the solution was removed for determination of specific activity. The rest of the solution was mixed with 9 mL of saline and passed through a sterile 0.2- μ m filter and collected in a vented sterile vial. The specific activity and radiochemical purity were determined by analytic HPLC (30% acetonitrile and 70% 0.1 mol/L ammonium formate, 2 mL/min).

^{11}C -GR89696 (the racemic tracer) and the ^{11}C -labeled inactive enantiomer, (+)- ^{11}C -GR89696, were similarly prepared starting from (\pm)-7 (the racemic precursor) and (+)-7 (the inactive isomer), respectively.

Baboon PET Studies

General Design. Three adult male baboons (baboons A, B, and C; 24, 13, and 14 kg, respectively) were studied in 10 separate PET experiments. The first aim was to characterize the brain uptake of ^{11}C -GR103545 under control and blocked conditions. Each baboon was studied in 2 PET experiments (i.e., 6 scans). The first experiment was a baseline scan with ^{11}C -GR103545 to establish the regional distribution of its specific binding. After this, the nonselective opiate receptor antagonist naloxone was administered in a dose of 1 mg/kg intravenously, to block specific binding of the tracer. This was followed by a second scan with ^{11}C -GR103545. The second aim was to evaluate the enantiomeric selectivity of the uptake. For this purpose, baboon A was studied in 4 PET experiments, the first with ^{11}C -GR89696, that is, the racemic tracer; the second with ^{11}C -GR89696 after pretreatment with naloxone, 1 mg/kg intravenously; the third with ^{11}C -GR103545, that is, the active optical isomer; and the fourth with (+)- ^{11}C -GR89696, that is, the inactive isomer.

PET Experimental Procedures. Experiments were performed according to protocols approved by the Columbia Presbyterian Medical Center Institutional Animal Care and Use Committee and previously described (36). In summary, unfed animals were immobilized with ketamine (10 mg/kg intramuscularly) and anesthetized with 1%–2% isoflurane in O_2 via an endotracheal tube. A catheter was inserted in a femoral artery for arterial blood sampling. PET was performed with the ECAT EXACT HR+ scanner (Siemens/CTI) in 3-dimensional mode. A 10-min transmission scan was obtained before radiotracer injection for attenuation correction. Radiotracers were administered by intravenous bolus injection over 30 s. Emission data were collected in 3-dimensional mode for 121 min as 24 successive frames of increasing duration (6×10 s, 2×1 min, 4×2 min, 2×5 min, 10×10 min).

Input Function Measurement. Procedures associated with measurement of the input function have previously been described in detail (36). In summary, arterial samples were collected every 10 s for the first 2 min and every 20 s from 2 to 4 min using an automated blood-sampling system and drawn manually thereafter at various intervals to a total of 30 samples. Six samples (collected at 2, 4, 12, 30, 60, and 90 min) were analyzed by HPLC to determine the fraction of plasma activity representing unmetabolized parent tracer. A biexponential function was fitted to the 6 measured parent fractions and used to interpolate values between and after the measurements. The input function was then calculated as the product of total counts and interpolated parent fraction at each time point. The measured input function values were fitted

to a sum of 3 exponentials and the fitted values were used as input for the kinetic analyses. The clearance of the parent tracer (L/h) was calculated as the ratio of the injected dose to the area under the curve of the input function. The initial distribution volume (V_{bol} , in L) was calculated as the ratio of the injected dose to peak plasma concentration. The plasma free fraction (f_1) was determined by ultrafiltration of triplicate 0.2-mL aliquots of plasma. The amount of radioactivity in the filter unit and the filtrate was counted. The f_1 was calculated as the ratio of the concentration (radioactivity/mL) of the filtrate to that of the total.

Image Analysis. An MR image of each baboon's brain was obtained to identify the regions of interest (ROIs), as previously described (36). The following regions were drawn on the MR images: cerebellum; brain stem; thalamus; striatum; medial temporal lobe; and temporal, cingulate, frontal, parietal, and occipital cortices.

PET emission data were attenuation corrected using the transmission scan, and frames were reconstructed using a Shepp filter (cutoff frequency of 0.5 cycles per projection ray). Reconstructed image files were then processed by MEDx image analysis software (Sensor System). Each baboon's PET images were coregistered with the corresponding MR image as previously described (36). ROI boundaries were transferred from the MR image to the individual registered PET frames, and time-activity curves were measured and decay corrected. Right and left regions were averaged. For a given animal, the same regions were used for all radiotracers.

Brain Uptake. Total brain uptake was expressed as the percentage of the injected dose per gram of tissue in a region encompassing the entire brain. Regional peak times were defined as the mid time of the frame associated with the highest activity value. To estimate the degree of washout from the brain captured during the scan (121 min), the decrease in activity from the peak to that recorded during the last frame of acquisition was calculated and expressed as a percentage of the peak activity.

Derivation of V_T . Regional total distribution volumes (V_T , in mL/g) were derived by kinetic analysis of the regional time-activity curves, using the metabolite-corrected arterial plasma concentrations as the input function, according to a 1- or 2-tissue-compartment model. Kinetic parameters (K_1 and k_2 for the 1-tissue-compartment model; K_1 – k_4 for the 2-tissue-compartment model) were derived by nonlinear regression using a Levenberg-Marquart least-squares minimization procedure implemented in MATLAB (The Math Works, Inc.). In the 1-tissue-compartment model, K_1 (mL/g/min) and k_2 (per min) are the rate constants governing the transfer of the ligands into and out of the brain, respectively. In the 2-tissue-compartment model, K_1 and k_2 are the rate constants governing the transfer of the ligands into and out of the nondisplaceable compartment (free and nonspecific binding), whereas k_3 (per min) and k_4 (per min) describe the respective rates of association to and dissociation from the receptors.

V_T was derived from kinetic parameters as:

$$V_T = \frac{K_1}{k_2} \quad \text{Eq. 1}$$

in the 1-tissue-compartment model, and as:

$$V_T = \frac{K_1}{k_2} \left(1 + \frac{k_3}{k_4} \right) \quad \text{Eq. 2}$$

in the 2-tissue-compartment model.

Analysis of the first 6 PET experiments showed that, using an unconstrained 2-tissue-compartment model, the Levenberg-Marquart algorithm failed for almost all regions in half the experiments, as some kinetic parameters assumed a negative value. Therefore, a constrained ($k > 0$) sequential quadratic programming algorithm (also implemented in MATLAB) was used. Given the unequal sampling over time (increasing frame acquisition time from the beginning to the end of the study), the least-squares minimization procedures were weighted by frame duration.

Derivation of κ -OR Parameters. Cerebellar V_T ($V_{T\text{ CER}}$) was used as an estimate of the nondisplaceable distribution volume (including free and nonspecific binding) in the ROIs. The binding potential (BP, in mL/g) was derived as the difference between V_T in the ROI ($V_{T\text{ ROI}}$) and $V_{T\text{ CER}}$. BP is related to receptor parameters by:

$$V_{T\text{ ROI}} - V_{T\text{ CER}} = \text{BP} = f_1 \times \frac{B_{\text{max}}}{K_D}, \quad \text{Eq. 3}$$

where B_{max} is the concentration of available sites (nmol/L/g of tissue) and K_D is the in vivo equilibrium dissociation constant of the radiotracer (nmol/L/ml of brain water) (37).

The main outcome measure of interest was the specific-to-nonspecific equilibrium partition coefficient (V_3''). V_3'' was calculated as the ratio of BP to $V_{T\text{ CER}}$ and related to receptor parameters by:

$$\frac{\text{BP}}{V_{T\text{ CER}}} = V_3'' = f_2 \times \frac{B_{\text{max}}}{K_D}, \quad \text{Eq. 4}$$

where f_2 is the free fraction in the nonspecific distribution volume of the brain ($f_2 = f_1/V_{T\text{ CER}}$) (37).

Statistical Analysis. Values are given as mean \pm SD. Dependant variables were analyzed using a paired t test, ANOVA, or repeated-measures ANOVA, when appropriate. Post hoc tests were performed using the Fisher test of protected least-significant difference. A 2-tailed probability value of 0.05 was selected as the significance level. Goodness of fit of models with different levels of complexity was compared using the Akaike information criterion and the F test. The SE of the parameters was given by the diagonal of the covariance matrix and expressed as a percentage of the parameters (coefficient of variation). Primary references have been published by Laruelle et al. (37).

RESULTS

Radiochemistry

The synthesis time for ^{11}C -GR103545 was about 50 min. Radiochemical yield (based on the amount of $^{11}\text{CO}_2$) at end of synthesis (EOS) was about 2%. Chemical purity was more than 95% and radiochemical purity was more than 98%.

PET Experiments

Injected Doses. Mean \pm SD and ranges of injected doses, specific activities at time of injections, and injected masses for the ^{11}C -GR103545 and ^{11}C -GR89696 scans ($n = 10$) were 107.3 ± 40.7 MBq (37.0–177.6 MBq), $9,916 \pm 5,069$ GBq/mmol (3,700–18,315 GBq/mmol), and 0.00025 ± 0.00011 mg/kg (0.00016–0.00051 mg/kg). Masses below 0.0003 mg/kg were generally without significant effects on

blood pressure, heart rate, respiratory rate, or recovery from anesthesia. Masses higher than 0.0003 mg/kg were limited to 2 scans blocked with naloxone, when potential physiologic side effects from κ -OR agonism were prevented.

Plasma Analysis. Plasma metabolite analysis after the injection of ^{11}C -GR103545 revealed no lipophilic metabolites. The fraction of total plasma activity corresponding to the parent compound at 2, 4, 12, 30, 60, and 90 min after injection of ^{11}C -GR103545 ($n = 4$ experiments) was $91\% \pm 10\%$, $83\% \pm 14\%$, $55\% \pm 12\%$, $35\% \pm 7\%$, $25\% \pm 5\%$, and $28\% \pm 9\%$, respectively. Initial distribution volume (V_{bal}) clearance, and f_1 for ^{11}C -GR103545 were 1.9 ± 0.5 L, 23.3 ± 8.6 L/h, and $24\% \pm 9\%$, respectively ($n = 4$ experiments).

Control Experiments. ^{11}C -GR103545 showed excellent brain penetration, with peak total brain uptake of $0.010\% \pm 0.004\%$ injected dose per gram at 16 ± 3 min ($n = 4$ experiments). Over time, activity became concentrated in regions with high κ -OR densities, that is, cingulate cortex, striatum, frontal cortex, temporal cortex, and parietal cortex. Intermediate levels were found in thalamus and medial temporal lobe, and low levels in brain stem and occipital cortex. Lowest levels were found in cerebellum (Fig. 3A). Figure 4 displays time-activity curves for a subset of representative brain regions (cerebellum, occipital cortex, frontal cortex, parietal cortex, and cingulate cortex) after administration of ^{11}C -GR103545. Good separation was seen between activities in different regions. In regions with lowest activity, initial uptake was rapid, with an early and sharp peak, followed by rapid washout. In regions with higher activity, uptake was slower, with smoother peaks, followed by moderate washout. Regional mean peak uptake times are presented in Table 1. Regional rank order for ^{11}C -GR103545 peak uptake time was cerebellum < occipital cortex < brain stem < thalamus = medial temporal lobe < temporal cortex < frontal cortex = parietal cortex < striatum < cingulate cortex. Rank order for the mean regional washout of ^{11}C -GR103545 (relative decrease from peak time to the last frame; Table 1) was cerebellum > occipital cortex > brain stem > temporal cortex > parietal cortex > thalamus = medial temporal lobe > frontal cortex > cingulate cortex = striatum.

The 4 ^{11}C -GR103545 baseline scans were chosen to assess the best model for kinetic analysis. In all regions, V_T was larger when calculated with a 2-tissue-compartment model than when calculated with a 1-tissue-compartment model, and this difference was statistically significant (repeated-measures ANOVA, effect of model $P \leq 0.0001$). There was no significant difference in the SE of V_T (percentage coefficient of variation) between the 2 models (repeated-measures ANOVA, effect of model $P = 0.07$). However, the goodness of fit to the data, as indicated by the Akaike information criterion, was significantly better for the 2-tissue-compartment model (repeated-measures ANOVA, effect of model $P \leq 0.0001$). Similarly, the F test indicated a significantly better fit ($P \leq 0.05$) for the 2-tissue-com-

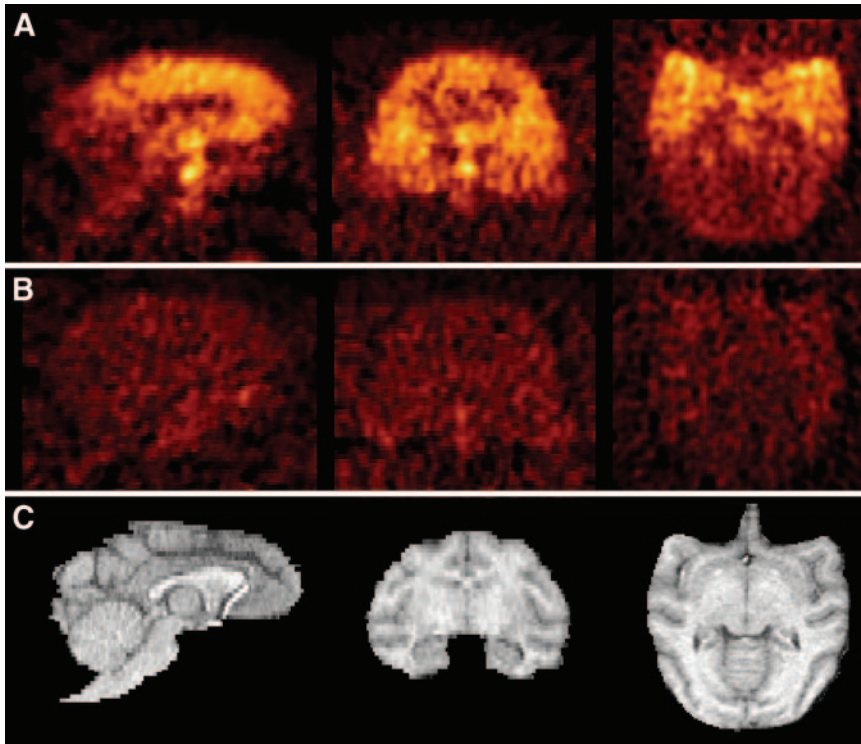


FIGURE 3. (A) Sagittal (left), coronal (middle), and transverse (right) slices of representative baboon PET scan acquired from 40 to 80 min after injection of ^{11}C -GR103545. Activity is concentrated in cingulate, frontal, temporal, and parietal cortices; medial temporal lobe; and striatum. Little activity is seen in brain stem and occipital cortex. Cerebellar uptake appears close to background level. (B) ^{11}C -GR103545 scans (same slices in same baboon over same interval) after pretreatment with naloxone, 1 mg/kg intravenously. Images in A and B are normalized to their respective injected doses of activity and displayed with same intensity range. (C) Coregistered MR images of same baboon.

partment model in all 4 studies for 6 of the 10 regions and in 3 of the 4 studies for the remaining 4 regions (Table 2). Moreover, mean regional F values were significantly different from unity (i.e., the null hypothesis of no difference in goodness of fit between 2-tissue-compartment model and 1-tissue-compartment model) by paired *t* test ($P = 0.02$). In

view of the significant difference in calculated V_T between the 2 models, and the significantly better fit to the data (Akaike information criterion and F test) of the 2-tissue-compartment model, the 2-tissue-compartment model was selected as the best model for the kinetic analysis of all ROIs, including the reference region (cerebellum).

Table 3 (baseline columns) displays the regional V_T , BP, and V_3'' values for ^{11}C -GR103545. The rank order for specific binding was cingulate cortex > striatum > frontal cortex > temporal cortex > parietal cortex > medial temporal lobe > thalamus > brain stem > occipital cortex.

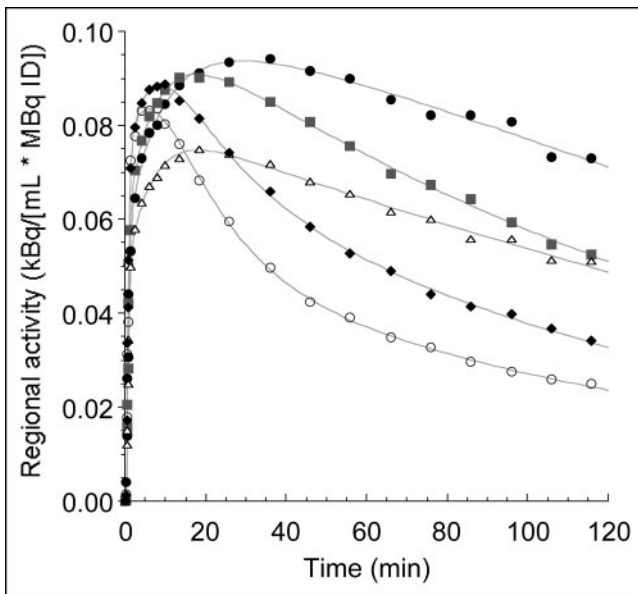


FIGURE 4. Time-activity curves in selected brain regions from single, representative study after bolus injection of ^{11}C -GR103545: cerebellar (○), occipital (◆), frontal (△), parietal (■), and cingulate (●). Points are measured values; lines are values fitted to a 2-tissue-compartment model. ID = injected dose.

TABLE 1

Regional Peak Uptake Times and Activity Washout for ^{11}C -GR103545

Region	Peak uptake time (min)	Activity washout (%)
Cerebellum	8.0 ± 1.6	66.1 ± 5.5
Brain stem	10.1 ± 6.1	46.8 ± 12.6
Thalamus	18.3 ± 11.9	33.1 ± 12.6
Striatum	38.5 ± 5.0	22.4 ± 5.8
Medial temporal lobe	18.3 ± 6.5	32.4 ± 8.8
Cingulate cortex	41.0 ± 12.9	22.6 ± 1.9
Frontal cortex	22.3 ± 4.3	26.5 ± 5.1
Temporal cortex	21.0 ± 6.1	37.2 ± 4.3
Parietal cortex	22.9 ± 6.3	34.4 ± 5.2
Occipital cortex	9.0 ± 1.2	56.5 ± 4.9

Values are mean ± SD of 4 experiments; activity washout is decrease from peak to last frame.

TABLE 2
Comparison of Compartment Models for ¹¹C-GR103545 Kinetic Analysis

Region	Model	V _T (mL/g)	SE (%CV)	Goodness of fit AIC	2TCM superior to 1TCM*
Cerebellum	1TCM	3.3 ± 0.6	3.6 ± 2.1	-78 ± 22	
	2TCM	3.6 ± 0.6	2.6 ± 2.4	-139 ± 25	4
Brain stem	1TCM	4.5 ± 2.6	3.2 ± 1.8	-86 ± 23	
	2TCM	5.0 ± 2.4	3.7 ± 2.9	-129 ± 16	4
Thalamus	1TCM	6.8 ± 3.0	2.9 ± 1.1	-83 ± 23	
	2TCM	7.2 ± 3.0	2.5 ± 1.4	-113 ± 23	3
Striatum	1TCM	10.2 ± 4.9	2.3 ± 1.0	-102 ± 32	
	2TCM	9.8 ± 4.9	2.7 ± 1.3	-117 ± 34	3
Medial temporal lobe	1TCM	6.2 ± 3.1	3.1 ± 1.4	-87 ± 23	
	2TCM	6.7 ± 3.1	3.3 ± 1.8	-113 ± 28	3
Cingulate cortex	1TCM	10.0 ± 5.3	2.9 ± 1.1	-88 ± 25	
	2TCM	10.5 ± 5.0	2.8 ± 1.6	-114 ± 40	3
Frontal cortex	1TCM	7.2 ± 3.4	2.8 ± 1.8	-98 ± 30	
	2TCM	7.9 ± 3.3	2.6 ± 2.2	-143 ± 25	4
Temporal cortex	1TCM	7.3 ± 3.7	2.5 ± 1.3	-90 ± 27	
	2TCM	7.7 ± 3.6	2.1 ± 1.5	-135 ± 22	4
Parietal cortex	1TCM	6.8 ± 3.2	1.6 ± 0.5	-101 ± 31	
	2TCM	7.2 ± 3.2	1.0 ± 0.3	-149 ± 25	4
Occipital cortex	1TCM	4.4 ± 2.2	2.9 ± 1.3	-79 ± 25	
	2TCM	4.8 ± 2.1	1.7 ± 1.1	-139 ± 25	4

*Number of studies (of 4) in which F test indicates significantly better fit ($P \leq 0.05$) for 2TCM than for 1TCM.

1TCM = 1-tissue-compartment model; 2TCM = 2-tissue-compartment model; AIC = Akaike information criterion.

Values are mean ± SD of 4 experiments. V_T is significantly larger with 2TCM (repeated-measures ANOVA, effect of model, $P \leq 0.0001$). Fit was significantly better (AIC more negative) with 2TCM (repeated-measures ANOVA, effect of model, $P \leq 0.0001$).

Values of V₃^{''} were above 0.5 for all regions except brain stem and occipital cortex. Specific binding was blocked by pretreatment with naloxone.

Blocking Experiments. After naloxone, 1 mg/kg intravenously (Table 3, after-naloxone columns, and Fig. 5), values of BP and V₃^{''} fell significantly (repeated-measures ANOVA, $P < 0.001$) across all regions to fairly homogeneous low-to-negligible levels. The change in V_T^{CER} after naloxone was not significant (from 3.7 to 3.4 mL/g; $P =$

0.77), supporting the absence of significant specific binding in that region.

Assessment of Enantiomeric Selectivity. Figure 6 displays brain time-activity curves for a subset of representative brain regions (cerebellum, occipital cortex, frontal cortex, parietal cortex, and cingulate cortex) for the 4 experiments performed on baboon A to compare the imaging properties of the racemic compound ¹¹C-GR89696 and its active (¹¹C-GR103545) and inactive ((+)-¹¹C-GR89696) enantiomers.

TABLE 3
¹¹C-GR103545 Binding Parameters at Baseline and After Naloxone

Region	V _T (mL/g)	Baseline (n = 3)		V _T (mL/g)	After naloxone (n = 3)	
		BP (mL/g)	V ₃ ^{''}		BP (mL/g)	V ₃ ^{''}
Cerebellum	3.7 ± 1.6	—	—	3.4 ± 1.2	—	—
Brain stem	5.1 ± 2.9	1.4 ± 1.3	0.3 ± 0.2	3.6 ± 1.8	0.3 ± 0.6	0.1 ± 0.2
Thalamus	6.9 ± 3.6	3.2 ± 2.1	0.8 ± 0.3	4.1 ± 2.1	0.8 ± 0.9	0.2 ± 0.2
Striatum	10.5 ± 5.9	6.8 ± 4.3	1.7 ± 0.5	4.7 ± 2.8	1.3 ± 1.5	0.3 ± 0.3
Medial temporal lobe	7.0 ± 3.8	3.3 ± 2.1	0.8 ± 0.2	4.0 ± 1.8	0.6 ± 0.6	0.2 ± 0.1
Cingulate cortex	10.9 ± 6.1	7.2 ± 4.5	1.9 ± 0.4	4.9 ± 2.3	1.6 ± 1.1	0.4 ± 0.1
Frontal cortex	8.5 ± 3.7	4.8 ± 2.1	1.3 ± 0.2	4.3 ± 2.3	1.0 ± 1.1	0.2 ± 0.2
Temporal cortex	8.1 ± 4.3	4.4 ± 2.7	1.1 ± 0.2	4.4 ± 2.1	1.0 ± 0.8	0.3 ± 0.1
Parietal cortex	7.5 ± 3.8	3.7 ± 2.2	1.0 ± 0.2	4.1 ± 2.2	0.7 ± 1.0	0.2 ± 0.2
Occipital cortex	4.9 ± 2.5	1.2 ± 0.9	0.3 ± 0.1	3.7 ± 1.7	0.3 ± 0.5	0.1 ± 0.1

Values are mean ± SD. Naloxone has no significant effect on V_T in CER ($P = 0.77$; paired *t* test). Effect of naloxone on regional V₃^{''} is highly significant (repeated-measures ANOVA, effect of condition, $P \leq 0.0001$).

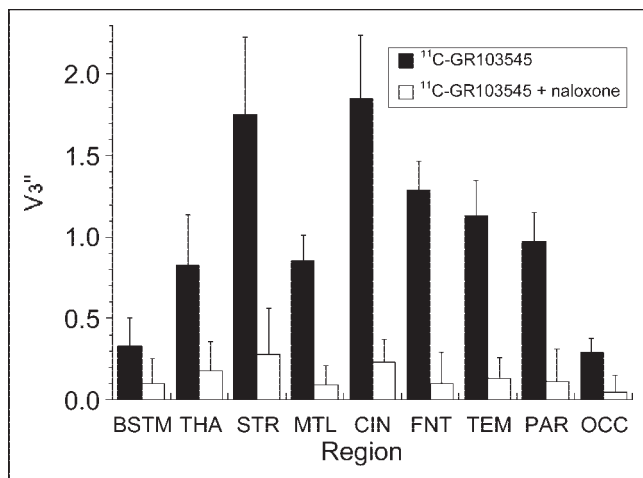


FIGURE 5. Mean regional V_3'' values for $^{11}\text{C-GR103545}$ at baseline and after pretreatment with naloxone, 1 mg/kg intravenously ($n = 3$). Error bars = SD. After naloxone, regional V_3'' values are significantly reduced (repeated-measures ANOVA, $P < 0.001$) and approach homogeneous low-to-negligible levels. BSTM = brain stem; THA = thalamus; STR = striatum; MTL = medial temporal lobe; CIN = cingulate cortex; FNT = frontal cortex; TEM = temporal cortex; PAR = parietal cortex; OCC = occipital cortex.

To facilitate comparison, activities displayed in Figure 6 are normalized to injected doses, and scales of the axes have been kept constant. All 3 compounds showed good brain penetration. Racemic $^{11}\text{C-GR89696}$ (Fig. 6A) showed moderate separation between activities in different regions. Initial uptake was rapid, with fairly early and sharp peaks, followed by moderate washout. After pretreatment with naloxone, $^{11}\text{C-GR89696}$ activity (Fig. 6B) peaked more rapidly, was followed by rapid washout, and showed little separation between regions. In comparison with the racemic $^{11}\text{C-GR89696}$, $^{11}\text{C-GR103545}$ (Fig. 6C) showed similar initial uptake, but more rapid washout in the region of reference (cerebellum). There was greater separation between regions, as well as smoother, more protracted peaks and slower washout in regions with highest activity, potentially predicting higher specific binding. In contrast, the inactive enantiomer (+)- $^{11}\text{C-GR89696}$ (Fig. 6D) showed sharp peaks, rapid washout, and minimal separation between regions. The time-activity curves were similar in appearance to those measured when the specific binding of $^{11}\text{C-GR89696}$ was blocked by naloxone (Fig. 6B).

Regional V_3'' values are shown in Table 4 for each of the 4 conditions. As predicted, V_3'' values were higher in all regions (by approximately 56%–200%) for $^{11}\text{C-GR103545}$ than for $^{11}\text{C-GR89696}$. For $^{11}\text{C-GR89696}$, V_3'' values were low or moderate across regions, with the highest value (cingulate cortex) not exceeding 1.0. This specific binding was almost entirely blocked by pretreatment with naloxone, 1 mg/kg intravenously, as indicated by values of V_3'' homogeneously close to zero. Similarly, (+)- $^{11}\text{C-GR89696}$ had only homogeneous, nonspecific uptake.

DISCUSSION

This paper has characterized $^{11}\text{C-GR103545}$, a novel radiotracer for imaging κ -OR with PET. $^{11}\text{C-GR103545}$ demonstrated the favorable characteristics required of a useful PET radiotracer (38).

The synthesis method reported here resulted in optical purity of the synthetically obtained GR103545 and its chiral precursor, (–)-7, and our measured optical rotations of GR103545 agreed with those reported in the literature (31,35). The radiosyntheses of $^{11}\text{C-GR103545}$, $^{11}\text{C-GR89695}$, and (+)- $^{11}\text{C-GR89695}$ previously reported used ^{11}C -methyl chloroformate and the corresponding precursors (34). Using this method, we found that the specific activities of all 3 tracers were relatively low (ranged from approximately 5,550 to 18,315 GBq/mmol EOS) in comparison to those achieved using ^{11}C -methyl iodide in our center (55.5–148.0 TBq/mmol EOS). A high specific activity will be important for human studies, as GR103545 is a potent κ -OR agonist. No pharmacologic effects of $^{11}\text{C-GR103545}$ were detected in the studies reported here.

Plasma metabolite analysis revealed no lipophilic metabolites having a propensity to diffuse into the brain. The metabolic rate was moderate, with 27% of unmetabolized parent remaining at 60 min after injection. f_1 was high enough (24%) to be measurable with conventional ultracentrifugation techniques. Thus, the input function could appropriately be characterized.

As predicted by its lipophilicity ($\log P = 3.14$), $^{11}\text{C-GR103545}$ shows excellent brain penetration. However, the nonspecific binding was relatively low, with a $V_{T\text{ CER}}$ value of 3.7 mL/g. Given an f_1 of 24%, a nonspecific distribution volume of 3.7 mL/g indicates that the free fraction in the nondisplaceable compartment is 6.4%, which is acceptable. The washout from the brain was fast enough to permit a practical scan duration (120 min in our experiments). The peak uptake of $^{11}\text{C-GR103545}$ in the highest uptake region (cingulate cortex) was achieved in about 40 min and showed 23% washout by the end of the scan (Table 1).

The regional uptake was amenable to quantitative analysis using compartmental modeling. Regional V_T was derived by kinetic analysis of the regional time-activity curves, using the metabolite-corrected arterial plasma concentrations as the input function, according to a 1-tissue-compartment model and a 2-tissue-compartment model. V_T was significantly larger when calculated with a 2-tissue-compartment model, and a 2-tissue-compartment model provided a significantly better fit to the data as indicated by both the Akaike information criterion and the F test (Table 2). The 2-tissue-compartment model was therefore selected as the best model for kinetic analysis of all ROIs, including the reference region (cerebellum). Using this model, regional V_T values were derived with appropriate confidence (percentage coefficient of variation < 3%; Table 2). The fact that a 2-tissue-compartment model was found to be superior in both receptor-rich and reference (cerebellum)

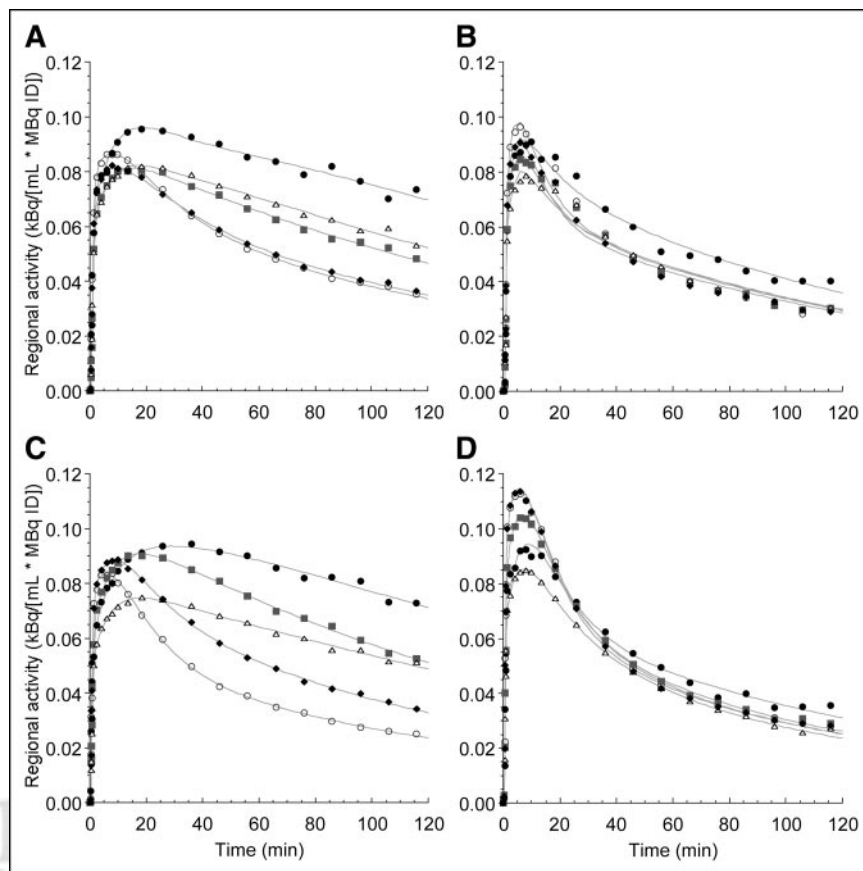


FIGURE 6. Time-activity curves in selected brain regions from 4 experiments performed on baboon A: cerebellar (○), occipital (◆), frontal (△), parietal (■), and cingulate (●). (A) Racemic ^{11}C -GR89696. (B) ^{11}C -GR89696 after pretreatment with naloxone. (C) The active enantiomer ^{11}C -GR103545. (D) The inactive enantiomer (+)- ^{11}C -GR89696. Points are measured values; lines are values fitted to a 2-tissue-compartment model. ID = injected dose.

regions does not necessarily imply the presence of a significant specific binding compartment in the cerebellum, as model order determination is not always based strictly on the presence or absence of receptors in a region. However, it may have implications for alternative methods for deriving receptor parameters. If the reference region is not parsimoniously fitted by a 1-tissue-compartment model, then fitting procedures based on this assumption and using reference tissue (as opposed to plasma) inputs may be prone to error (39).

The derivation of receptor parameters requires determination of the specific and nonspecific components of the regional distribution volume. The most practical method to derive these contributions is to use V_T in a region of reference (i.e., a region devoid of significant receptor density) as an estimate of the nonspecific distribution volume. Despite the fact that low density of κ -OR has been reported in the cerebellum (6,40), its use as a region of reference was validated in this study. First, blocking the κ -OR with naloxone failed to significantly affect ^{11}C -GR103545 $V_{T,CER}$,

TABLE 4
Assessment of Enantiomeric Selectivity

Region	V_3'' value			
	^{11}C -GR89696	^{11}C -GR89696 after naloxone	^{11}C -GR103545	(+)- ^{11}C -GR89696
Brain stem	0.21	-0.02	0.33	-0.03
Thalamus	0.53	0.15	1.30	0.09
Striatum	0.75	0.08	1.65	0.07
Medial temporal lobe	0.34	0.10	0.68	0.03
Cingulate cortex	1.00	0.19	1.67	0.13
Frontal cortex	0.42	-0.02	0.82	-0.11
Temporal cortex	0.56	0.11	0.93	0.02
Parietal cortex	0.30	-0.02	0.90	0.01
Occipital cortex	0.02	-0.04	0.32	0.00

Each of the 4 conditions represents results of single PET experiment on same baboon ($n = 4$ scans).

indicating that the contribution of saturable binding to ^{11}C -GR103545 $V_{\text{T CER}}$ was negligible. Second, under blocking conditions, $V_{\text{T ROI}}$ values were comparable to $V_{\text{T CER}}$ (Table 3 and Fig. 5).

The regional pattern of ^{11}C -GR103545 specific binding found in baboons in this study agrees strongly with the regional distribution of κ -OR demonstrated in the nonhuman primate brain in *in vitro* and autoradiography studies (6,7), supporting the κ -OR-selective profile of ^{11}C -GR103545 as a radiotracer. Thus, ^{11}C -GR103545 specific binding was highest in cingulate cortex, striatum, frontal cortex, temporal cortex, and parietal cortex; intermediate levels were found in thalamus and medial temporal lobe; and low levels in brain stem and occipital cortex. In addition, the regional pattern of ^{11}C -GR103545 specific binding is quite different from that of ^{11}C -carfentanil, a μ -OR-selective radiotracer, again supporting a non- μ -OR profile for ^{11}C -GR103545. Figure 7 compares regional baseline V_3'' values for ^{11}C -GR103545 ($n = 4$) with regional V_3'' values for ^{11}C -carfentanil ($n = 9$) acquired in our laboratory in the same baboons and using the same ROIs. For ^{11}C -carfentanil, V_3'' values are highest in thalamus and striatum; moderate in medial temporal lobe and brain stem; and low in cingulate cortex, frontal cortex, temporal cortex, and parietal cortex. Specific binding is negligible in occipital cortex, which is commonly used as a region of reference for this tracer. Thus, regions with high or moderate ^{11}C -GR103545 V_3'' values (e.g., cingulate cortex, frontal cortex, temporal cortex, and parietal cortex) have low ^{11}C -carfentanil V_3'' values. Conversely, the region with highest ^{11}C -carfentanil V_3'' (thalamus) has only moderate ^{11}C -GR103545 specific binding. Additional competition experiments, using κ -selective agents, are required to further establish the *in vivo* selectivity of the specific binding of ^{11}C -GR103545 for κ -OR.

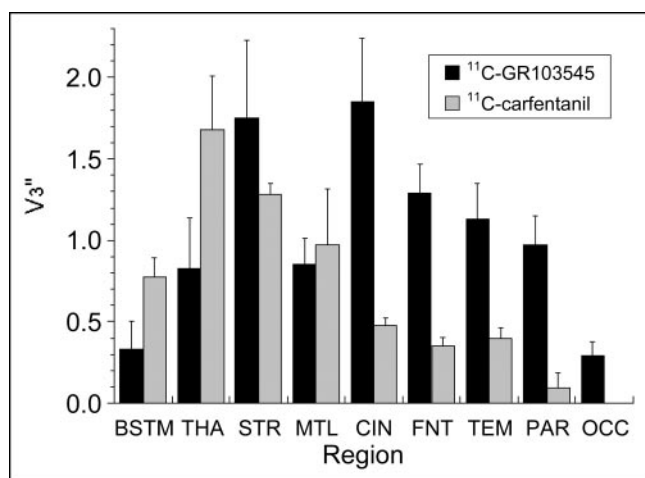


FIGURE 7. Comparison between ^{11}C -GR103545 ($n = 3$) and ^{11}C -carfentanil ($n = 9$) regional V_3'' values in same baboons. BSTM = brain stem; THA = thalamus; STR = striatum; MTL = medial temporal lobe; CIN = cingulate cortex; FNT = frontal cortex; TEM = temporal cortex; PAR = parietal cortex; OCC = occipital cortex.

However, to date, *in vivo* pharmacology studies in rhesus monkeys have revealed only potent κ -OR-mediated agonist effects of GR89696 in behavioral, respiratory, and neuroendocrine assays (33).

The ^{11}C -GR103545 BP values derived in this study are consistent with expectations derived from the literature. For example, the B_{max} of κ -OR in human cortex is approximately 50 fmol/mg (cingulate gyrus, 68 fmol/mg; inferior, medial, and superior temporal gyri, 50 fmol/mg; superior parietal cortex, 35 fmol/mg; inferior, medial, and superior frontal gyri, 51 fmol/mg) (4). Taking these literature B_{max} values, the mean values of ^{11}C -GR103545 BP in the corresponding regions in our study (cingulate cortex, 7.2 mL/g; temporal cortex, 4.4 mL/g; parietal cortex, 3.7 mL/g; frontal cortex, 4.8 mL/g; Table 3), and the f_1 value of 24%, the equation $\text{BP} = f_1 \times B_{\text{max}}/K_D$ estimates *in vivo* K_D values from each of the 4 regions. The estimated K_D values derived from cingulate cortex, temporal cortex, parietal cortex, and frontal cortex are 2.3, 2.3, 2.55, and 2.7 nmol/L, respectively, giving a mean ^{11}C -GR103545 K_D value of 2.5 nmol/L *in vivo* in the baboon. This value is relatively consistent with the *in vitro* values: racemic GR89696 displaces ^3H -bremazocine binding with a K_i of 2.3 nmol/L in the guinea pig (32) and 1.15 nmol/L in the rhesus monkey (33). Experiments conducted at low specific activities would be required to formally derive the *in vivo* K_D of ^{11}C -GR103545. These experiments were not conducted, because of concerns about the potent κ -OR agonist effect of the compound.

The specific-to-nonspecific partition coefficient at equilibrium, V_3'' , is an important parameter in the initial evaluation of a potential radiotracer, as it provides a measure of the signal-to-noise ratio associated with derivation of receptor parameters. Generally, V_3'' equal to or greater than 0.5 is desirable for reliable quantification (38). ^{11}C -GR103545 achieved a V_3'' higher than 0.5 in all regions examined, with the exception of brain stem and occipital cortex, where the density of κ -OR may be too low to be measured reliably with this tracer. The improvement in V_3'' achieved by using the pure active enantiomer rather than the racemic mixture was significant. For ^{11}C -GR89696, V_3'' values were low or moderate across regions, with only the cingulate cortex and striatum being much above 0.5 and the highest value (cingulate cortex) not exceeding 1.0 (Table 4). Thus, compared with ^{11}C -GR89696, ^{11}C -GR103545 provided an enhanced signal-to-noise ratio that should significantly improve the reliability of the measurements.

CONCLUSION

^{11}C -GR103545 was shown to be a promising radioligand for imaging κ -OR with PET. The rate of metabolism was moderate and the free fraction was relatively high, both of which are important factors for the measurement of input function. Brain uptake displayed appropriate kinetics, with significant washout observed within the time frame of the

PET experiment. Brain uptake was significantly reduced under blocking conditions. Regional V_T values could be derived with appropriate confidence using a 2-tissue-compartment model. The use of $V_{T\text{ CER}}$ as an estimate of the nondisplaceable distribution volume was validated. The magnitude and regional distribution of BP were consistent with expectations from the literature. V_3'' values were predictive of reliable quantification in most ROIs. Thus, ^{11}C -GR103545 satisfies several important criteria for further development and evaluation in humans.

ACKNOWLEDGMENTS

The authors thank Harry Acosta, Mohammed Ali, John Castrillon, Elizabeth Hackett, Van Phan, Nurat Quadri, and Lyudmilla Savenkova for their excellent technical assistance. This study was supported by the Public Health Service (1 R21MH/DA66505-01, 1-K02-MH01603-01) and the Lieber Center for Schizophrenia Research at Columbia University.

REFERENCES

- Dhawan B, Cesslin F, Raghuram R, et al. Classification of opioid receptors. *Pharmacol Rev.* 1996;48:567–592.
- Minami M, Satoh M. Molecular biology of the opioid receptors: structures, functions and distributions. *Neurosci Res.* 1995;23:121–145.
- Simonin F, Gaveriaux-Ruff C, Befort K, et al. Kappa-opioid receptor in humans: cDNA and genomic cloning, chromosomal assignment, functional expression, pharmacology, and expression pattern in the central nervous system. *Proc Natl Acad Sci USA.* 1995;92:7006–7010.
- Hiller JM, Fan LQ. Laminar distribution of the multiple opioid receptors in the human cerebral cortex. *Neurochem Res.* 1996;21:1333–1345.
- Peckys D, Landwehrmeyer GB. Expression of mu, kappa, and delta opioid receptor messenger RNA in the human CNS: a 33P in situ hybridization study. *Neuroscience.* 1999;88:1093–1135.
- Slater P, Cross AJ. Autoradiographic distribution of dynorphin1–9 binding sites in primate brain. *Neuropeptides.* 1986;8:71–76.
- Ko MC, Lee H, Harrison C, et al. Studies of micro-, kappa-, and delta-opioid receptor density and G protein activation in the cortex and thalamus of monkeys. *J Pharmacol Exp Ther.* 2003;306:179–186.
- Kim KW, Eun YA, Soh SM, Eun JS, Cho KP. Ligand binding profiles of U-69,593-sensitive and -insensitive sites in human cerebral cortex membranes: evidence of kappa opioid receptors heterogeneity. *Life Sci.* 1996;58:1671–1679.
- Butelman ER, Ko MC, Sobczyk-Kojiro K, et al. Kappa-opioid receptor binding populations in rhesus monkey brain: relationship to an assay of thermal antinociception. *J Pharmacol Exp Ther.* 1998;285:595–601.
- Caudle RM, Finegold AA, Mannes AJ, Tobias MD, Kenshalo DR Jr, Iadarola MJ. Spinal kappa1 and kappa2 opioid binding sites in rats, guinea pigs, monkeys and humans. *Neuroreport.* 1998;9:2523–2525.
- Raynor K, Kong H, Chen Y, et al. Pharmacological characterization of the cloned kappa-, delta-, and mu-opioid receptors. *Mol Pharmacol.* 1994;45:330–334.
- Jordan BA, Devi LA. G-protein-coupled receptor heterodimerization modulates receptor function. *Nature.* 1999;399:697–700.
- Richardson A, Demoliou-Mason C, Barnard EA. Guanine nucleotide-binding protein-coupled and -uncoupled states of opioid receptors and their relevance to the determination of subtypes. *Proc Natl Acad Sci U S A.* 1992;89:10198–10202.
- Rusovici DE, Negus SS, Mello NK, Bidlack JM. Kappa opioid receptors are differentially labeled by arylacetamides and benzomorphans. *Eur J Pharmacol.* 2004;485:119–125.
- Mello NK, Negus SS. Interactions between kappa opioid agonists and cocaine: preclinical studies. *Ann N Y Acad Sci.* 2000;909:104–132.
- de Lanerolle NC, Williams A, Meredith C, et al. Dynorphin and the kappa 1 ligand [^3H]U69,593 binding in the human epileptogenic hippocampus. *Epilepsy Res.* 1997;28:189–205.
- Chappell PB, Leckman JF, Scahill LD, Hardin MT, Anderson G, Cohen DJ. Neuroendocrine and behavioral effects of the selective kappa agonist spiradoline in Tourette's syndrome: a pilot study. *Psychiatry Res.* 1993;47:267–280.
- Mathieu-Kia AM, Fan LQ, Kreek MJ, Simon EJ, Hiller JM. Mu-, delta- and kappa-opioid receptor populations are differentially altered in distinct areas of postmortem brains of Alzheimer's disease patients. *Brain Res.* 2001;893:121–134.
- Sheffler DJ, Roth BL. Salvinorin A: the "magic mint" hallucinogen finds a molecular target in the kappa opioid receptor. *Trends Pharmacol Sci.* 2003;24:107–109.
- Berger PA, Watson SJ, Akil H, Barchas JD. The effects of naloxone in chronic schizophrenia. *Am J Psychiatry.* 1981;138:913–918.
- Vink R, Portoghese PS, Faden AI. Kappa-opioid antagonist improves cellular bioenergetics and recovery after traumatic brain injury. *Am J Physiol.* 1991;261:R1527–R1532.
- Dannals RF, Ravert HT, Frost JJ, Wilson AA, Burns HD, Wagner HN Jr. Radiosynthesis of an opiate receptor binding radiotracer: [^{11}C]carfentanil. *Int J Appl Radiat Isot.* 1985;36:303–306.
- Frost J, Mayberg H, Sadzot B, et al. Comparison of [^{11}C]diprenorphine and [^{11}C]carfentanil binding to opiate receptors in humans by positron emission tomography. *J Cereb Blood Flow Metab.* 1990;10:484–492.
- Lever J, Mazza S, Dannals R, Ravert H, Wilson A, Wagner H. Facile synthesis of [^{11}C]buprenorphine for positron emission tomographic studies of opioid receptors. *Int J Rad Appl Instrum [A].* 1990;41:745–752.
- Theodore W, Carson R, Andreasen P, et al. PET imaging of opiate receptor binding in human epilepsy using [^{18}F]cyclofoxy. *Epilepsy Res.* 1992;13:129–139.
- Lever JR, Scheffel U, Kinter CM, et al. In vivo binding of N1'-(^{11}C)methyl-naltrindole to delta-opioid receptors in mouse brain. *Eur J Pharmacol.* 1992;216:459–460.
- Birch PJ, Rogers H, Hayes AG, et al. Neuroprotective actions of GR89696, a highly potent and selective kappa-opioid receptor agonist. *Br J Pharmacol.* 1991;103:1819–1823.
- Rogers H, Birch PJ, Harrison SM, et al. GR94839, a kappa-opioid agonist with limited access to the central nervous system, has antinociceptive activity. *Br J Pharmacol.* 1992;106:783–789.
- Hayes AG, Birch PJ, Hayward NJ, et al. A series of novel, highly potent and selective agonists for the kappa-opioid receptor. *Br J Pharmacol.* 1990;101:944–948.
- Herrero JF, Headley PM. Functional evidence for multiple receptor activation by kappa-ligands in the inhibition of spinal nociceptive reflexes in the rat. *Br J Pharmacol.* 1993;110:303–309.
- Naylor A, Judd D, Lloyd J, Scopes D, Hayes A, Birch P. A potent new class of kappa-receptor agonist: 4-substituted 1-(arylacetyl)-2-[(dialkylamino)methyl]piperazines. *J Med Chem.* 1993;36:2075–2083.
- Caudle RM, Mannes AJ, Iadarola MJ. GR89,696 is a kappa-2 opioid receptor agonist and a kappa-1 opioid receptor antagonist in the guinea pig hippocampus. *J Pharmacol Exp Ther.* 1997;283:1342–1349.
- Butelman ER, Ko MC, Traynor JR, Vivian JA, Kreek MJ, Woods JH. GR89,696: a potent kappa-opioid agonist with subtype selectivity in rhesus monkeys. *J Pharmacol Exp Ther.* 2001;298:1049–1059.
- Ravert HT, Mathews WB, Musachio JL, Scheffel U, Finley P, Dannals RF. [^{11}C]methyl 4-[(3,4-dichlorophenyl)acetyl]-3-[(1-pyrrolidinyl)-methyl]-1-piperazinecarboxylate ([^{11}C]GR89696): synthesis and in vivo binding to kappa opiate receptors. *Nucl Med Biol.* 1999;26:737–741.
- Ravert HT, Scheffel U, Mathews WB, Musachio JL, Dannals RF. [(11)C]-GR89696, a potent kappa opiate receptor radioligand: in vivo binding of the R and S enantiomers. *Nucl Med Biol.* 2002;29:47–53.
- Huang Y, Hwang DR, Narendran R, et al. Comparative evaluation in nonhuman primates of five PET radiotracers for imaging the serotonin transporters: [^{11}C]McN 5652, [^{11}C]ADAM, [^{11}C]DASB, [^{11}C]DAPA, and [^{11}C]AFM. *J Cereb Blood Flow Metab.* 2002;22:1377–1398.
- Laruelle M, Baldwin R, Rattner Z, et al. SPECT quantification of [^{123}I]iomazenil binding to benzodiazepine receptors in nonhuman primates. I. Kinetic modeling of single bolus experiments. *J Cereb Blood Flow Metab.* 1994;14:439–452.
- Laruelle M, Slifstein M, Huang Y. Relationships between radiotracer properties and image quality in molecular imaging of the brain with positron emission tomography. *Mol Imaging Biol.* 2003;5:363–375.
- Slifstein M, Laruelle M. Models and methods for derivation of in vivo neuroreceptor parameters with PET and SPECT reversible radiotracers. *Nucl Med Biol.* 2001;28:595–608.
- Schadrack J, Willoch F, Platzer S, et al. Opioid receptors in the human cerebellum: evidence from [^{11}C]diprenorphine PET, mRNA expression and autoradiography. *Neuroreport.* 1999;10:619–624.